A Swept-Sine-Type Single Measurement to Estimate Intermodulation Distortion in a Dynamic Range of Audio Signal Amplitudes

Pietro Burrascano, Alessandro Terenzi, Stefania Cecchi, *Member, IEEE*, Matteo Ciuffetti, and Susanna Spinsante, *Senior Member, IEEE*

***Abstract*— In the world of real audio systems, it is extremely important to model and identify their nonlinear behavior, especially in the case of professional audio devices. In this context, it is useful to have a quantitative estimation of the nonlinearity degree of the device, which can be obtained by exploiting an efficient and rapid measurement methodology. In this article, we propose an original estimation technique targeting the third-order intermodulation distortion (IMD) and based on a single detection. The proposed technique can be implemented both on devices operating in baseband and in bandpass. Starting from the same single detection, the technique allows to give either an estimate of the third-order IMD for the signal level actually used and to extrapolate the estimate of the IMD to signal levels different from the one actually used. Experimental verifications on real audio devices have allowed to validate the procedure in operational situations, thus confirming the validity of the proposed approach.**

***Index Terms*— Audio system, Hammerstein system, intermodulation distortion (IMD) measurement, nonlinear device, pulse compression.**

I. Introduction

IN THE world of nonlinear audio devices, an important aspect is the system modeling. Knowledge of the system model allows to compensate for the nonlinear behavior of the device, such as a loudspeaker [1], [2] or Hi-Fi systems [3], by developing an inverse filter of the nonlinear model, or to emulate nonlinear audio devices with particular attention to vacuum tube-based ones, such as amplifiers and guitar pedal distortion effects [4]–[8]. Furthermore, increasingly accurate models of these systems are made feasible by the enormous computing power available nowadays. The availability of high computing power at low cost makes it possible to carry out model identification procedures even using portable devices, designed to operate outside traditional laboratories, which can provide preliminary estimates of models and distortion levels by measurements carried out directly in the operational context in which the system under test is used. In this perspective, it becomes a priority to have estimation methods that minimize the duration of the testing phase.

During years, many approaches have been proposed for nonlinear modeling, which can be grouped into three main categories, i.e., the white-box approaches, gray-box approaches, and black-box approaches. The difference between these three categories is related to the level of physical knowledge of the real system, which is necessary to adopt a specific technique. White-box approaches required a complete knowledge of the nonlinear system. These techniques exploit wave digital filters [9], [10] or differential equations [11] to obtain a complete model of the real system. Even if the obtained model is highly accurate, complete knowledge of the physical system is not always possible. For this reason, the gray- and black-box approaches have been developed, which, respectively, require only partial knowledge of the system or only the knowledge of input and output signals [12]–[14]. Gray-box approaches use the input–output (I/O) relationship to identify the system, and then, the model is improved using the block diagram of the circuit. Two examples can be found in [15] and [16], where a dynamic range compression system has been modeled using a gray-box approach with an iterative parameter optimization procedure. Speaking of black-box approaches, these are the most widely adopted since they do not require any previous knowledge of the system. Some of the most well-known models, such as the Volterra filters [17], belong to the category of black-box approaches. These filters are derived from the Volterra series, to which truncation is applied, because of the infinite number of terms. Moreover, even with the reduced Volterra series, the number of coefficients needed to define the model quickly becomes very large as the degree of nonlinearity increases. This is a serious limitation since it allows the identification of systems with only a moderate degree of nonlinearity. Research studies have been focused on simplified Volterra series expansion models [18]. Among them, the Hammerstein and Wiener models rely on splitting the linear dynamic part from the static, nonlinear

Manuscript received February 25, 2021; revised April 10, 2021; accepted April 24, 2021. Date of publication May 6, 2021; date of current version May 24, 2021. This work was supported in part by the University of Perugia through its program for Basic Research, in 2019 and 2020 and in part by the Marche Region in Implementation of the Financial Program POR MARCHE FESR 2014–2020, Project Marche Innovation and Research Facilities for Connected and Sustainable Living Environments ("Miracle"), CUP under Grant B28I19000330007. The Associate Editor coordinating the review process was Priya Ranjan Muduli. *(Corresponding author: Alessandro Terenzi.)*

Pietro Burrascano and Matteo Ciuffetti are with the Department of Engineering, Universitá di Perugia, 06123 Terni, Italy (e-mail: pietro.burrascano@unipg.it; matteo.ciuffetti@studenti.unipg.it).

Alessandro Terenzi, Stefania Cecchi, and Susanna Spinsante are with the Department of Information Engineering, Universitá Politecnica delle Marche, 60131 Ancona, Italy (e-mail: a.terenzi@staff.univpm.it; s.cecchi@staff.univpm.it; s.spinsante@staff.univpm.it).

Digital Object Identifier 10.1109/TIM.2021.3077983

one. Although less general than Volterra or Wiener filters, the Hammerstein and Wiener models provide accurate modeling of even strong nonlinearities, using a reduced number of parameters [12], [14]. Several efforts have been made in the literature to develop an algorithm for identifying such models, mainly exploiting a suitable input swept-sine signal [19]–[22]. The main difference between the Wiener and the Hammerstein models is how the nonlinear and the linear part are placed. For the Hammerstein model, the nonlinear static part is placed before the linear one [23]–[26], whereas for the Wiener model, the opposite happens, i.e., the nonlinear part follows the linear one [23], [25]. Finally, for the Wiener–Hammerstein model, two linear parts are present and placed before and after the nonlinear one [23], [27]. Other notable black-box approaches use neural networks to obtain the nonlinear model of the real system [28], [29]. The choice of the proper model is related to the type of system that has to be modeled and to the computational power that is available for the identification and emulation process. The main purpose of these models is to represent as completely as possible the operation of the nonlinear system.

In parallel to this overall representation of the I/O behavior of the system, it is also useful to have global parameters that give a quantitative numerical measurement of the degree of nonlinearity of the system [30]. The definition of these parameters requires to specify the measurement conditions, the type of excitation signal adopted, and the nonlinear structure model. In this context, total harmonic distortion (THD) and the kth harmonic distortion (HD_k) have been defined using as excitation signal a pure tone in order to evaluate the generation of higher order harmonics of the system. Despite that these two parameters are good distortion indicators, the simplicity of the adopted excitation signal led to some limitations, e.g., it is not possible to estimate how the system manages complex signals featuring more than one harmonic. For this reason, it is important to introduce a more advanced distortion parameter, i.e., the intermodulation distortion (IMD). It is calculated exploiting an excitation signal of higher complexity generated by overlapping two oscillating signals at different frequencies and considering one of the intermodulation components generated by the simultaneous presence of these two signals in the nonlinear system. In a previous work [31], we have proposed a technique for estimating the second-order IMD, particularly suitable in the case of baseband systems, i.e., when extends down to frequencies close to the dc, such as the audio field. Other intermodulation components can be used to characterize the degree of nonlinearity: these choices, which are applicable in any context, are particularly useful when the band of the system is relatively narrow, so that the second intermodulation component would fall below the useful operating range of the system and would be greatly attenuated, making its measurement impractical. An intermodulation component widely used in these cases is the third component (i.e., $2f_2 - f_1$), whose values fall in or close to the useful band of the system, if the ratio between the two frequency values f_1 and f_2 is close to the unit.

In this work, an innovative procedure for the estimation of the third-order intermodulation component, which extends the technique already proposed in [31], is presented. In particular, different from [31], we show that the availability of the nonlinear structure model, besides allowing the estimation of the IMD for one single amplitude of the input signal, also allows to perform extrapolations of the estimate in the case of excitation signals of amplitudes different from the one actually used in the measurement. This is an important aspect since the level of distortion is obviously related to the amplitude of the input signal. This technique, which we call *extrapolation* in this work, allows the estimation of the IMD parameter in a wide dynamic range of amplitudes by performing a single measurement, with a great advantage in terms of measurement execution time.

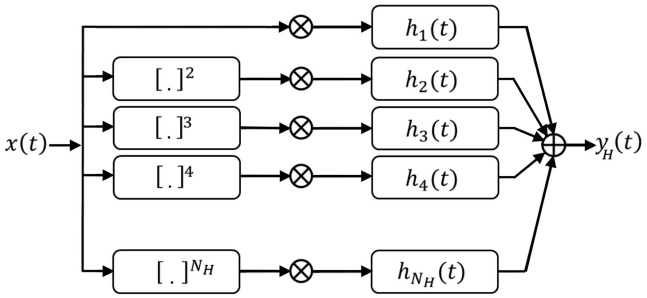

Fig. 1. Generalized polynomial Hammerstein model scheme, where the symbol $\otimes$ indicates convolution and the symbol $\oplus$ indicates the sum operation. The model is composed of N_H parallel branches, each of them consisting of a static nonlinearity followed by a linear filter.

This article is organized as follows. Section II explains the theoretical aspects of the procedure. Section III shows the experimental measurements carried out on real devices, and the results are obtained. Finally, Section IV reports conclusions and future work.

II. Derivation of the Estimation Procedure

Before presenting the derivation of the estimation procedure, the reader is advised that vectors and matrices will be denoted by square brackets.

We assume that the nonlinear system is validly represented through its Hammerstein model of order N_H, whose structure is shown in Fig. 1. The corresponding I/O relationship is

$$\begin{aligned} y_H(t) &= h_1(t) \otimes x(t) + h_2(t) \otimes x^2(t) + \cdots + h_{N_H}(t) \otimes x^{N_H}(t) \\ &= [x^j(t)]^T \otimes [h(t)] \end{aligned} \tag{1}$$

where the symbol $\otimes$ indicates convolution, $h_j(t)$, with $j = 1 \ldots N_H$, are the kernels that identify the model of the nonlinear system considered, and the vector $[h(t)]$ of dimension N_H, according to the notation adopted here, contains the ordered sequence of $h_j(t)$. Suppose that the input is an harmonic signal whose peak amplitude is R

$$x(t) = R\cos(\phi(t)) \tag{2}$$

and whose instantaneous angular frequency $\omega(t)$ is variable in time

$$\omega(t) = \frac{d\phi(t)}{dt}. \tag{3}$$

Combining (1) and (2) and relying on the Chebyshev polynomials [32], we can express the harmonics $\cos(j \cdot \phi(t))$ as a function of the powers $(\cos(\phi(t)))^j$

$$\begin{aligned}[\cos(j \cdot \phi(t))] &= [A_C][\cos(\phi(t))]^j \\ &= [A_C][R_C]^{-1}[R\cos(\phi(t))]^j \end{aligned} \tag{4}$$

where the entries of matrix $[A_C]$ are the coefficients of the Chebyshev polynomials of the first kind and $[R_C]$ is the diagonal matrix in which the term of index $\{i, i\}$ is the ith power of the amplitude R. Using the inverse of (4), the output of the Hammerstein model $y_H(t)$ can be expressed as follows:

$$\begin{aligned} y_H(t) &= [[R\cos(\phi(t))]^j]^T \otimes [h(t)] \\ &= [[R_C][A_C]^{-1}\cos(j \cdot \phi(t))]^T \otimes [h(t)] \\ &= [\cos(j \cdot \phi(t))]^T [[R_C][A_C]^{-1}]^T \otimes [h(t)] \\ &= [\cos(j \cdot \phi(t))]^T \otimes ([[A_C]^{-1}]^T [R_C])[h(t)] \\ &= [\cos(j \cdot \phi(t))]^T \otimes [g(t)], \end{aligned} \tag{5}$$

where

$$[g(t)] = ([[A_C]^{-1}]^T [R_C])[h(t)]. \tag{6}$$

The $g_j(t)$ functions are contained in the vector $[g(t)]$ in an ordered fashion. Expression (5) shows that, when $x(t) = R\cos(\phi(t))$, (1) can be modified in order to formulate the output signal $y_H(t)$ as a function of the harmonics of $x(t)$ rather than its powers. Then, (5) shows that the $g_j(t)$ functions are linearly related to the functions $h_j(t)$ associated with the powers of the same input signal as reported in (6). On the basis of the above formulation, a procedure for the identification of the Hammerstein model has been proposed; it assumes that the harmonic excitation signals are of the exponential swept-sine type and that they comply with specific constraints on their instantaneous phase [19], [22], [33]. The identification procedure involves the use of a filter, matched to the function given in (2), whose impulse response $\psi(t)$ is such that its convolution with the exponential swept-sine signal $x(t)$ produces a band-limited approximation of Dirac's delta function $\delta(t)$. By filtering the output of Hammerstein model $y_H(t)$ through $\psi(t)$, we get the output signal $u(t)$

$$\begin{aligned} u(t) &= y_H(t) \otimes \psi(t) \\ &= [\cos(j \cdot \phi(t))]^T \otimes [g(t)] \otimes \psi(t) \\ &= [\hat{\delta}(t)]^T \otimes [g(t)] \end{aligned} \tag{7}$$

where each element in $[\hat{\delta}(t)]$ is the band-limited approximation of the Dirac $\delta(t)$ function delayed by a quantity $\Delta t_k = L \ln(k)$ associated with the kth-order harmonic

$$[\hat{\delta}(t)] = \begin{bmatrix} \hat{\delta_1}(t + \Delta t_1) \\ \hat{\delta_2}(t + \Delta t_2) \\ \cdot \\ \hat{\delta_{N_H}}(t + \Delta t_{N_H}) \end{bmatrix}. \tag{8}$$

The parameter $L = \ln(f_{\mathrm{MAX}}/f_{\mathrm{MIN}})/T$ defines the variation rate over time of the instantaneous frequency of the exponential swept-sine signal, which sweeps between f_{MIN} and f_{MAX} in a time T. In (7), it is shown that the signal $u(t)$, output of the matched filter, consists of the sequence of the $g_j(t)$ functions, associated with delays Δt_k whose values differ only as a consequence of the order of the harmonic to which they are associated; the functions $g_j(t)$ have thus the meaning of pulse responses associated with the harmonics of the input signal. Moreover, if the parameter L is large enough to keep $g_j(t)$ apart, each of the $g_j(t)$ functions can be taken directly as a portion of $u(t)$ starting at a time instant identified by Δt_k.

Starting from the Fourier transforms $[G(f)]$ of the functions $g_j(t)$, it is possible to estimate the THD(f) associated with the system model and the single harmonic distortions HD$_k(f)$ [22], [34]. Moreover, from the knowledge of the $g_\alpha(t)$ functions produced by an R_α amplitude harmonic signal, this same formulation based on the Hammerstein model makes it possible to obtain the functions $g_\beta(t)$ associated with the harmonics that would be produced at the output of the given system, if it were excited by an R_β amplitude harmonic signal. In fact, based on the linear link between $[h(t)]$ and $[g(t)]$ defined by (6), we can write

$$[h(t)] = [R_\alpha]^{-1}[A_c]^T[g_\alpha(t)] \tag{9}$$

and based on the knowledge of the kernels $[h(t)]$ estimated from the $[g_\alpha(t)]$, we can obtain $[g_\beta(t)]$

$$\begin{aligned}[g_\beta(t)] &= ([[A_c]^{-1}]^T[R_\beta])\ [h(t)] \\ &= [[A_c]^{-1}]^T[R_\beta]\ [R_\alpha]^{-1}[A_c]^T[g_\alpha(t)]. \end{aligned} \tag{10}$$

This latter result allows to extrapolate the value of the harmonic distortion (THD or HD$_k$) associated with a (virtual) R_β amplitude input signals, starting from the $[g_\alpha(t)]$ functions obtained in correspondence to the input signal of amplitude R_α actually used in the measurements.

All the considerations made above rely on the functional connection between the harmonics of the input signal and its integer powers. If the input signal is characterized, at any given time instant, by a single instantaneous frequency (both in the case of sinusoidal and swept-sine signal), this functional connection is regulated by the matrix $[A_c]$, whose coefficients are those of Chebyshev's polynomials of the first kind, as in (4). If the input signal to the system is not characterized by a single instantaneous frequency, such as the swept-sine signal $\cos(\phi(t))$, but it is a more complex signal, the link between its powers and the corresponding harmonic components will be regulated by a relationship different from the previous one; it will still be a linear relationship since the Hammerstein model is linear in its parameters, but the matrix that relates the signal powers and its harmonic components will be different from $[A_c]$. The entries of the new matrix will be directly related to the specific input signal chosen; in fact, the harmonics generated as a consequence of a multifrequency input signal depend on both the nonlinear system and the complexity of the input signal, as all the possible intermodulation combinations between the single harmonic components of the input signal are generated. Our goal is to be able to use the Hammerstein model of the nonlinear system to estimate the IMD$_{(2f_2-f_1)}(f)$ that is generated at frequency $2f_2 - f_1$, if the input multifrequency harmonic signal $x(t)$ is of the type

$$x_{\omega_1,\omega_2}(t) = R(\cos(\omega_1 t) + \cos(\omega_2 t)). \tag{11}$$

We also want to show that, once identified the Hammerstein model of the nonlinear system, we can estimate the $\mathrm{IMD}_{(2f_2-f_1)}(f)$ that would be generated if the input signal had an amplitude $R = R_\beta$ different from the amplitude $R = R_\alpha$ of the signal $x_{\omega_1,\omega_2}(t)$ actually used in the identification phase. To obtain these results, we need to find the matrix that puts in correspondence the harmonics of the input signal $x_{\omega_1,\omega_2}(t)$ with its integer powers $[x_{\omega_1,\omega_2}(t)]^k$, in the case of the specific signal of (11), used to estimate the $\mathrm{IMD}_{(2f_2-f_1)}(f)$.

The signal we used in the present work, in analogy with what we did in [31], is the superimposition of two exponential swept-sine signals, both characterized by the same parameters but translated in time by a delay Δt. At any given time instant, the signal input to the system will therefore contain two harmonic components: the frequency of each of them evolves exponentially and the ratio of the two frequencies is constant throughout the duration of the double exponential swept-sine signal. If the identified Hammerstein model is of order N_H, we will have as many kernels in the vector $[h(t)]$; we must find the linear relationships that link the elements of the vector $[h(t)]$ that identifies the model to the elements of the vector $[g(t)]$ of dimension N_H, in which each kernel $g_{m,n}(t)$ is associated with the intermodulation frequency $mf_1 + nf_2$, $\{m, n\} \in \mathbb{Z}$. We are not interested in all the intermodulation frequencies that can be generated; in our case, we are interested in the IMD at frequency $2f_2 - f_1$, whose estimation requires knowledge of the components $g_{(2f_2-f_1)}(t)$, $g_{f_1}(t)$, and $g_{f_2}(t)$. In fact, we can write

$$\mathrm{IMD}_{(2f_2-f_1)}(f)\% = \frac{G_{(2f_2-f_1)}(f)}{G_{f_1}(f) + G_{f_2}(f)} \cdot 100 \tag{12}$$

where the functions $G_{m,n}(f)$ are the Fourier transform of the kernels $g_{m,n}(t)$. The overall vector must be of order N_H; thus, if our objective is to estimate the $\mathrm{IMD}_{(2f_2-f_1)}(f)$, the three kernels $g_{(2f_2-f_1)}(t)$, $g_{f_1}(t)$, and $g_{f_2}(t)$ must certainly be included in the vector $[g_{m,n}(t)]$. There is no rule to identify the additional kernels to be included in the vector $[g_{m,n}(t)]$, except that of verifying the linear independence of the resulting equations, in order to guarantee the compatibility of the system of equations and the invertibility of the coefficient matrix obtained. In this work, we have chosen to consider intermodulation components of the lowest order possible, which are usually those with relatively higher energy content. We report below the matrix $[A_{\mathrm{IMD}}]$ used in our experiments, associated with a model of order $N_H = 9$, with vector $[g_{m,n}(t)]$ defined as follows:

$$[g_{m,n}(t)] = \begin{bmatrix} g_{f_1}(t) \\ g_{f_2-f_1}(t) \\ g_{2f_1}(t) \\ g_{2f_2-f_1}(t) \\ g_{3f_1}(t) \\ g_{2f_2-2f_1}(t) \\ g_{4f_1}(t) \\ g_{3f_2-2f_1}(t) \\ g_{5f_1}(t) \end{bmatrix} \tag{13}$$

that relates to the vector $[h(t)]$ through

$$[g_{m,n}(t)] = [A_{\mathrm{IMD}}][R_c][h(t)] \tag{14}$$

in which $[R_c]$ and $[h(t)]$ have the meanings seen above and

$$[A_{\mathrm{IMD}}] = \begin{bmatrix} 1 & 0 & \frac{9}{4} & 0 & \frac{25}{4} & 0 & \frac{1225}{64} & 0 & \frac{3969}{64} \\ 0 & 1 & 0 & 3 & 0 & \frac{75}{8} & 0 & \frac{245}{8} & 0 \\ 0 & \frac{1}{2} & 0 & 2 & 0 & \frac{225}{32} & 0 & \frac{49}{2} & 0 \\ 0 & 0 & \frac{3}{4} & 0 & \frac{25}{8} & 0 & \frac{735}{64} & 0 & \frac{1323}{32} \\ 0 & 0 & \frac{1}{4} & 0 & \frac{25}{16} & 0 & \frac{441}{64} & 0 & \frac{441}{16} \\ 0 & 0 & 0 & \frac{3}{4} & 0 & \frac{15}{4} & 0 & \frac{245}{16} & 0 \\ 0 & 0 & 0 & \frac{1}{8} & 0 & \frac{9}{8} & 0 & \frac{49}{8} & 0 \\ 0 & 0 & 0 & 0 & \frac{5}{8} & 0 & \frac{245}{64} & 0 & \frac{567}{32} \\ 0 & 0 & 0 & 0 & \frac{1}{16} & 0 & \frac{49}{64} & 0 & \frac{81}{16} \end{bmatrix} \tag{15}$$

The matrix $[A_{\mathrm{IMD}}]$ has been obtained by developing the function $\{R(\cos(\omega_1 t)+\cos(\omega_2 t))\}^j$ raised to power up to index $j = N_H$ (in the case of the matrix $[A_{\mathrm{IMD}}]$ shown above up to $N_H = 9$) and regrouping, for each intermodulation harmonic present in the vector $[g_{m,n}(t)]$, the coefficients of the development referring to the frequency of that harmonic. It is useful to note that, having chosen as input a signal $x(t)$ for which the ω_1 and ω_2 angular frequency components have the same amplitude R, their role will be interchangeable, and the coefficients of the respective harmonics will be equal to each other. Consequently, to avoid linear dependence between equations of the system, the function $g(t)$ related only to one of the two angular frequencies has been inserted in the vector (13). The matrix $[A_{\mathrm{IMD}}]$ therefore plays, in the case that the input signal is a double exponential swept-sine signal, a role similar to that played by $[[A_c]^{-1}]^T$ in the case of the single exponential swept-sine signal [22]. Using the $[A_{\mathrm{IMD}}]$ matrix, we can retrace the steps previously seen for that case. By inverting (14), we obtain the expression of the vector $[h(t)]$ as a function of the kernels associated with the selected intermodulation components

$$[h(t)] = [R_c]^{-1}[A_{\mathrm{IMD}}]^{-1}[g_{m,n}(t)]. \tag{16}$$

Of particular interest here is the possibility of estimating the kernels $[g_{m,n}(t)|_{\beta}]$ that would be produced if the double exponential swept-sine input signal had an $R = R_\beta$ amplitude different from $R = R_\alpha$ actually used in the model identification phase; the starting data are the kernels $[g_{m,n}(t)|_{\alpha}]$ obtained in correspondence to an R_α amplitude. It is easily obtained

$$\begin{aligned}[g_{m,n}(t)|_{\beta}] &= [A_{\mathrm{IMD}}][R_\beta][h(t)] \\ &= [A_{\mathrm{IMD}}][R_\beta]\{[R_\alpha]^{-1}[A_{\mathrm{IMD}}]^{-1}[g_{m,n}(t)|_{\alpha}]\}.\end{aligned} \tag{17}$$

The experiments carried out in the following paragraph are based on the technique of estimating IMD $\mathrm{IMD}_{(2f_2-f_1)}(f)$

based on swept-sine pulse compression for the identification of the Hammerstein model of each of the physical systems considered. The IMD $\mathrm{IMD}_{(2f_2-f_1)}(f)$ was therefore estimated both in correspondence to the actual R_α amplitude value of the chirp signal used and referring to a hypothetical amplitude R_β based on the measurements made, in reality, with chirp of amplitude R_α. All swept-sine pulse compression-based estimates are compared with estimates from $\mathrm{IMD}_{(2f_2-f_1)}(f)$ obtained from the measurements based on the international norms.

III. Experimental Results

A. Experimental Setup

Several experiments were carried out to test the proposed approach to measure $\mathrm{IMD}_{(2f_2-f_1)}(f)$, analyzing different scenarios. In particular, two real-word audio devices were tested to analyze the results obtained by means of the proposed method. The results were compared to those obtained with the National Instruments sound and vibration toolkit [35], taken as the reference measurement system. The latter provides the possibility of measuring $\mathrm{IMD}_{(2f_2-f_1)}(f)$, according to the international standard [36]. A National Instruments PXI chassis (PXIe-1073) equipped with the PXI-4461 dynamic signal acquisition module [37], and connected to a desktop PC, was used for the signal's generation and acquisition. A LabVIEW script has been developed to manage the whole procedure. All the measurements were performed by setting a sampling frequency of 196 kHz and repeated at various frequencies in order to obtain an estimation of the distortion parameters in the frequency range from 1.5 to 15 kHz. For the $\mathrm{IMD}_{(2f_2-f_1)}(f)$ measurement, the frequency range of interest was divided into frequency intervals of 125 Hz width; for each of the 109 intervals identified, a signal was generated consisting of the superposition of two sinusoidal tones of amplitude R and frequencies $f_1 = f_0 - (\Delta\omega/2)$ and $f_2 = f_0 + (\Delta\omega/2)$, adjacent to the nominal frequency f_0, with $\Delta\omega = 80$ Hz as suggested from the International Electrotechnical Commission (IEC) standard. For the approach herein proposed, the same frequency range has been considered using the following parameters for the chirp generation:

1) $f_{\mathrm{start}} \rightarrow 185$ Hz;
2) $f_{\mathrm{stop}} \rightarrow 19\,000$ Hz;
3) Single chirp amplitude $\rightarrow 0.5$ a.u.;
4) Measurement band $\rightarrow [1500, 15\,000]$ Hz;
5) Chirp duration $\rightarrow 4.44$ s;
6) Sample frequency $\rightarrow 196\,000$ Hz;

Fig. 4 shows the flowchart of the two measurement procedures under comparison. Focusing on the IEC procedure shown in the left side, it requires a single measurement for each frequency and amplitude of input signal at which the distortion has to be estimated. The parameter *Step* allows to modify the number of measurement points between f_{start} and f_{stop}. On the right side, considering the proposed approach, a single measurement is able to estimate the distortion within the whole frequency range between f_{start} and f_{stop}.

Several experiments on synthetic and real devices have been performed. For the sake of brevity, Section III-B will report estimation measurement results focused on real audio devices, while Section III-C will report results on robustness study considering both a synthetic system and a real device.

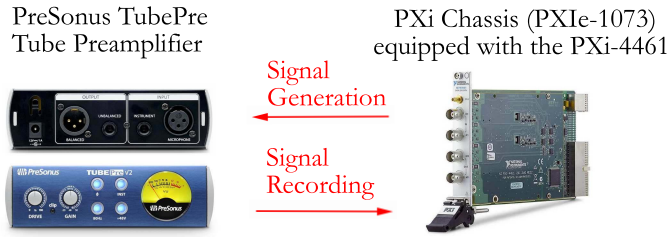

Fig. 2. Hardware connection for the real experiment considering the PreSonus TubePre preamplifier.

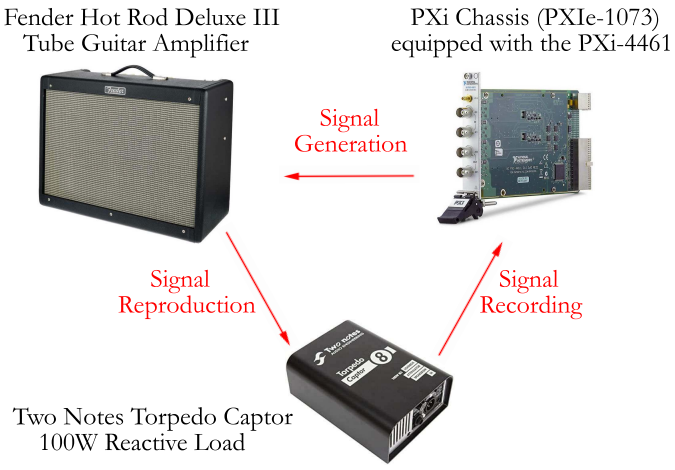

Fig. 3. Hardware connection for the real experiment considering the Fender Hot Rod Deluxe III amplifier.

B. Experiments on Real Devices

Two different devices under test (DUTs) were used in our experiments: a tube preamplifier and a guitar amplifier. The former, namely the PreSonus TubePre, is a microphone and instruments preamplifier, equipped with a 12AX7 triode valve. The device has been connected directly to the PXI-4461 acquisition board, as reported in Fig. 2. For this experiment, the two main controls of the preamplifier have been used, i.e., the drive that acts on the valve saturation and the gain control that acts on the overall gain. They have been set to 3 and 0 dB, respectively, to obtain a low level of nonlinearity, as reported in the experiments. The latter device, namely the Fender Hot Rod Deluxe III guitar amplifier, is a 40-W AB Class tube amplifier. The hardware connection is shown in Fig. 3. The amplifier was connected to the PXI-4461 acquisition board for the signal generation. For this experiment, the clean channel of the amplifier has been used, which has a single control, namely the volume, which acts on both the distortion and the output level of the amplifier; for the experiments, the volume has been set to a value of 2. The internal loudspeaker has been disconnected and the power output of the amplifier has been connected to a reactive load, in order to measure only the amplifier distortion, without including the nonlinearity of

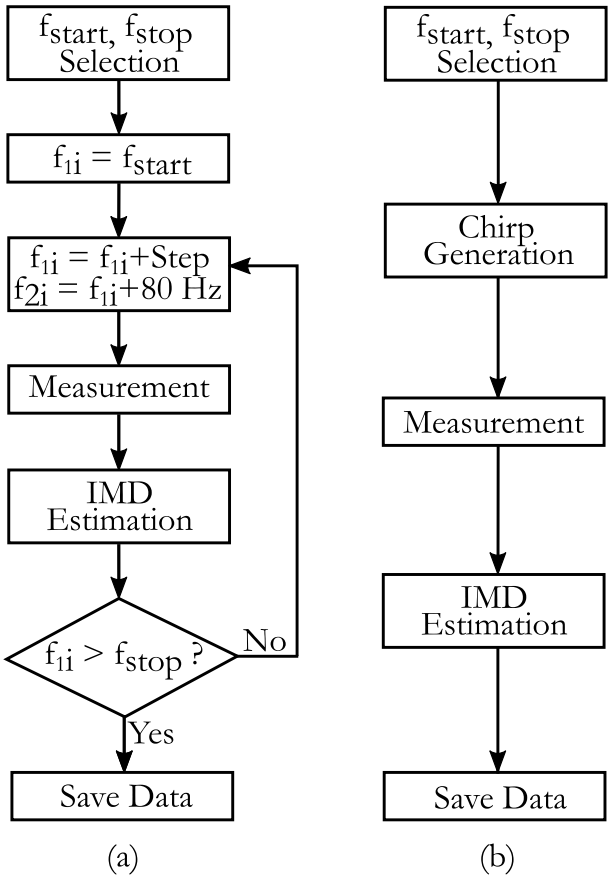

Fig. 4. Sequence of operations in the measurement procedure according to (a) IEC standard reference and (b) proposed approach.

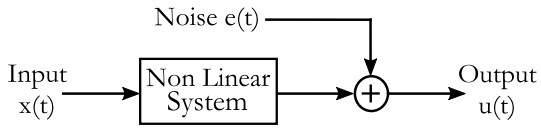

Fig. 5. Noise added to measurements for the robustness study.

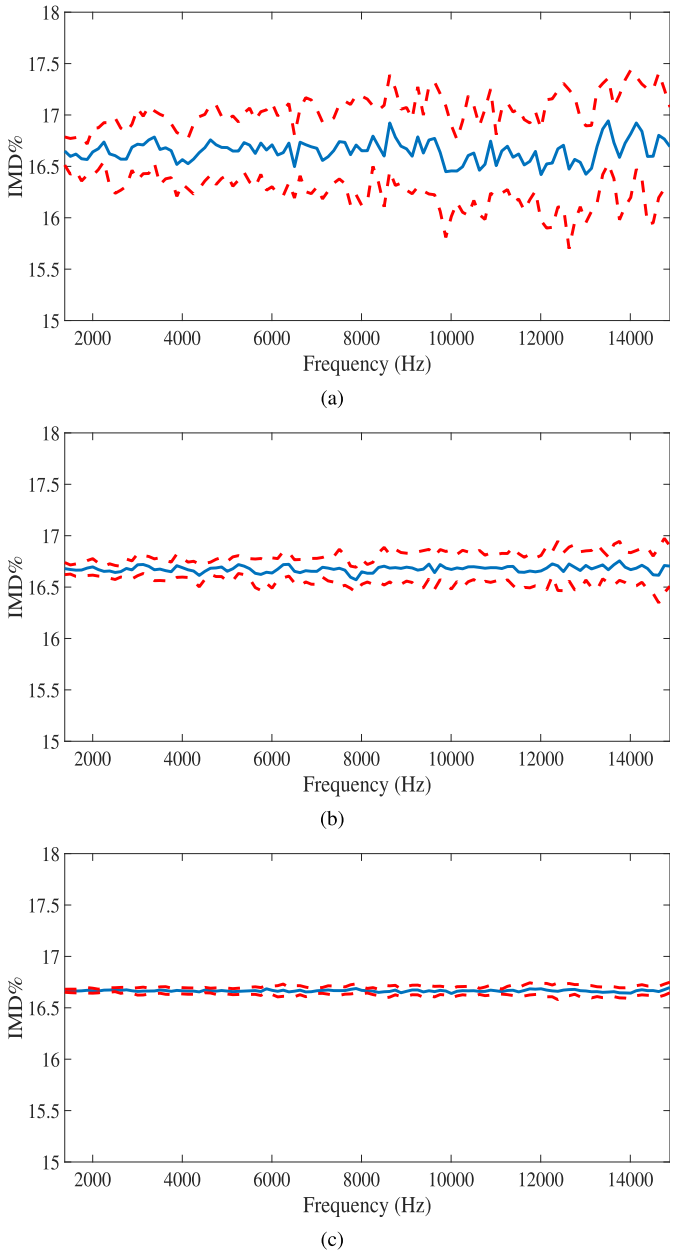

Fig. 6. Estimation results considering an input signal of 1.40 V_{pp} to synthetic polynomial nonlinearity. Dashed lines show the confidence interval for each measurement with a different SNR. In particular, (a) with a SNR of 10 dB, (b) with a SNR of 20 dB, and (c) with a SNR of 30 dB.

the loudspeaker. For the reactive load, a Two Notes Torpedo Captor has been used, a 100-W reactive load, specific for use with guitar amplifier having the same nominal impedance of the loudspeaker, i.e., 8 Ω. The reactive load has an output line that has been connected to the PXI-4461 input.

Figs. 8 and 9 show both the results for the first experiment on real devices, i.e., the PreSonus TubePre, considering a low level of nonlinearity and two amplitudes of input signal, i.e., 0.62 V_{pp} (peak-to-peak) and 1.40 V_{pp}. Each panel of the two figures compares the estimated (or extrapolated) trend, on solid blue lines, with the trend obtained through the technique indicated by the international standard, drawn with a red dashed line. Taking into consideration the $IMD_{(2f_2-f_1)}(f)$ measurement, the proposed approach shows very good estimation results in comparison to the standard IEC 60 268 methodology. As far as the extrapolation results are concerned, we focus on the results obtained for the 0.62-V_{pp} input signal, the first considered experiment is shown in Fig. 8(a), where the green dotted curve shows the estimated distortion without extrapolation; in this case, the two estimations are almost identical on the whole frequency band. Dealing with the extrapolated estimations, the results are shown in Fig. 8(b)–(d) on blue solid curves; in this case, the estimates show a good accuracy in the range between 1 and 8 kHz, in the upper range of frequencies (i.e., between 8 and 15 kHz), the estimates differ to a greater extent, although at a level still acceptable as an indication. Focusing on the results for the estimation with the 1.40-V_{pp} input signal, Fig. 9(a) shows the estimates behavior with no extrapolation in green dotted lines: the two curves are almost identical. The estimation with the extrapolated curves is shown in Fig. 9(b)–(d), where it gives useful indications on which are the trends of the IMD

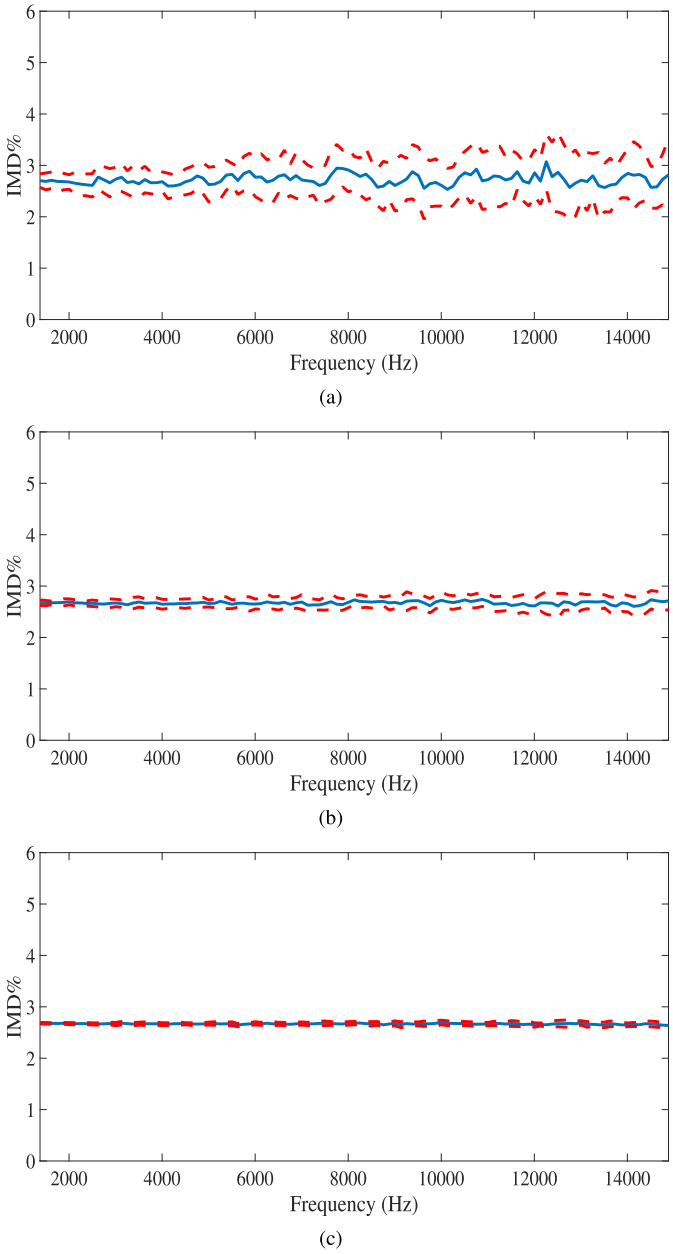

Fig. 7. Estimation results considering an input signal of 1.40 V_{pp} to the tube preamplifier. Dashed lines show the confidence interval for each measurement with a different SNR. In particular, (a) with a SNR of 10 dB, (b) with a SNR of 20 dB, and (c) with a SNR of 30 dB.

when the amplitude of the input signal is varied. Table I shows the percent mean difference between the proposed approach and the IEC 60 268 measurement method average on the entire frequency range, for all the estimations presented in Figs. 8 and 9. The results in both the estimation and extrapolation cases are good and show a very small difference between the proposed approach and the IEC measurements.

Focusing on the second experiment, i.e., with the Fender Hot Rod Deluxe III guitar amplifier, results are shown in Figs. 10 and 11, considering two amplitude values of the input signal, again 0.62 and 1.40 V_{pp}. Focusing on the experiments with 0.62-V_{pp} input signal, results are shown in Fig. 10. Fig. 10(a) shows the estimation with no extrapolation, the green dotted curve, which is almost overlapped

TABLE I

MEAN PERCENT DIFFERENCE BETWEEN $IMD_{(2f_2-f_1)}$ ESTIMATES AND THE VALUES OBTAINED BY THE METHOD PRESCRIBED BY IEC 60 268: PRESONUS TUBE PREAMPLIFIER EXPERIMENT. VALUES IN BOLD INDICATE ESTIMATES WITH NO EXTRAPOLATION

Input signal amplitude (V)	Considered amplitude (V)	Δ_{IMD} %
0.62	0.10	0.01
	0.18	0.01
	0.28	0.04
	0.62	**0.01**
1.40	0.41	0.03
	0.62	0.11
	0.93	0.12
	1.40	**0.01**

TABLE II

MEAN PERCENT DIFFERENCE BETWEEN $IMD_{(2f_2-f_1)}$ ESTIMATES AND THE VALUES OBTAINED BY THE METHOD PRESCRIBED BY IEC 60 268: FENDER HOT ROD DELUXE III AMPLIFIER EXPERIMENT. VALUES IN BOLD INDICATE ESTIMATES WITH NO EXTRAPOLATION

Input signal amplitude (V)	Considered amplitude (V)	Δ_{IMD} %
0.62	0.10	0.05
	0.18	0.12
	0.28	0.10
	0.62	**0.05**
1.40	0.41	0.17
	0.62	0.08
	0.93	0.22
	1.40	**0.07**

to the one obtained with the IEC procedure, in blue solid lines. Fig. 10(b)–(d) shows the extrapolated curves on blue lines; in this case, the standard measurement shows some oscillations that are not present in the extrapolated curves. The curves couples relative to the same amplitude of the input signal, however, have an extremely similar trend, both globally considering the distortion values, more in detail, if the frequency trend is considered. In Fig. 11, the results for the 1.40-V_{pp} input signal are visible. Focusing on the nonextrapolated estimation in Fig. 11(a), the curves couples have an almost identical shape. Extrapolated estimations are shown in Fig. 11(b)–(d); as for the estimation with 0.62-V_{pp} signal, oscillations are present, but, again, the two curves are comparable, with some difference only in Fig. 11(d), where the proposed approach seems to overestimate the behavior of the amplifier in the range between 4 and 12 kHz. Table II shows the percent mean difference between the proposed approach and the one defined in IEC 60 268, evaluated for all the estimations presented in Figs. 10 and 11. As for the Tube Pre case, the proposed approach gives an estimation of the IMD parameter value very close to the one of the IEC procedure. Comparing the two experiments, we can say that in both cases, the estimation of the IMD frequency curve is excellent. Slightly different are the results obtained for the extrapolation of the estimate of the third-order IMD, in which the results obtained with the first experiment are more adherent to the IEC measurements than in the case of the Fender amplifier;

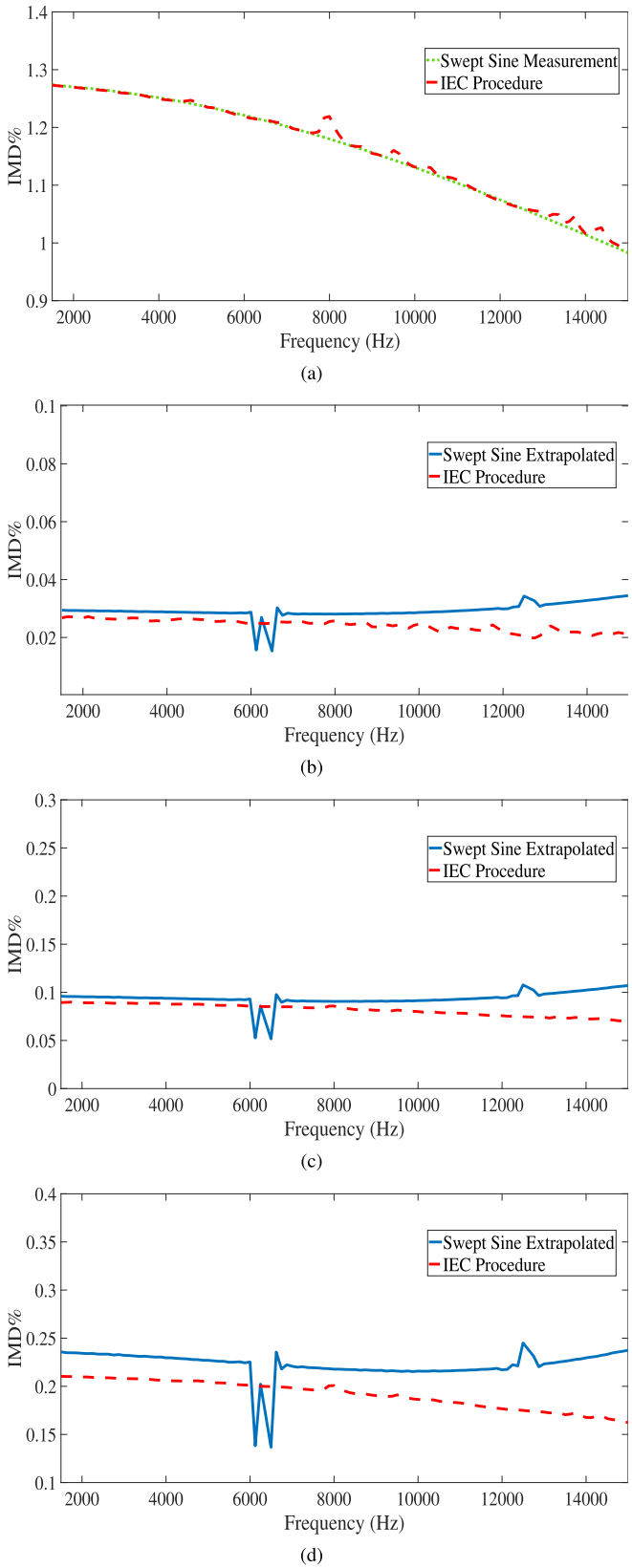

Fig. 8. Estimation results considering an input signal of 0.62 V_{pp} to the tube preamplifier. (a) Estimated curve, (b) with an extrapolation to 0.1 V, (c) with an extrapolation to 0.18 V, and (d) with an extrapolation to 0.28 V.

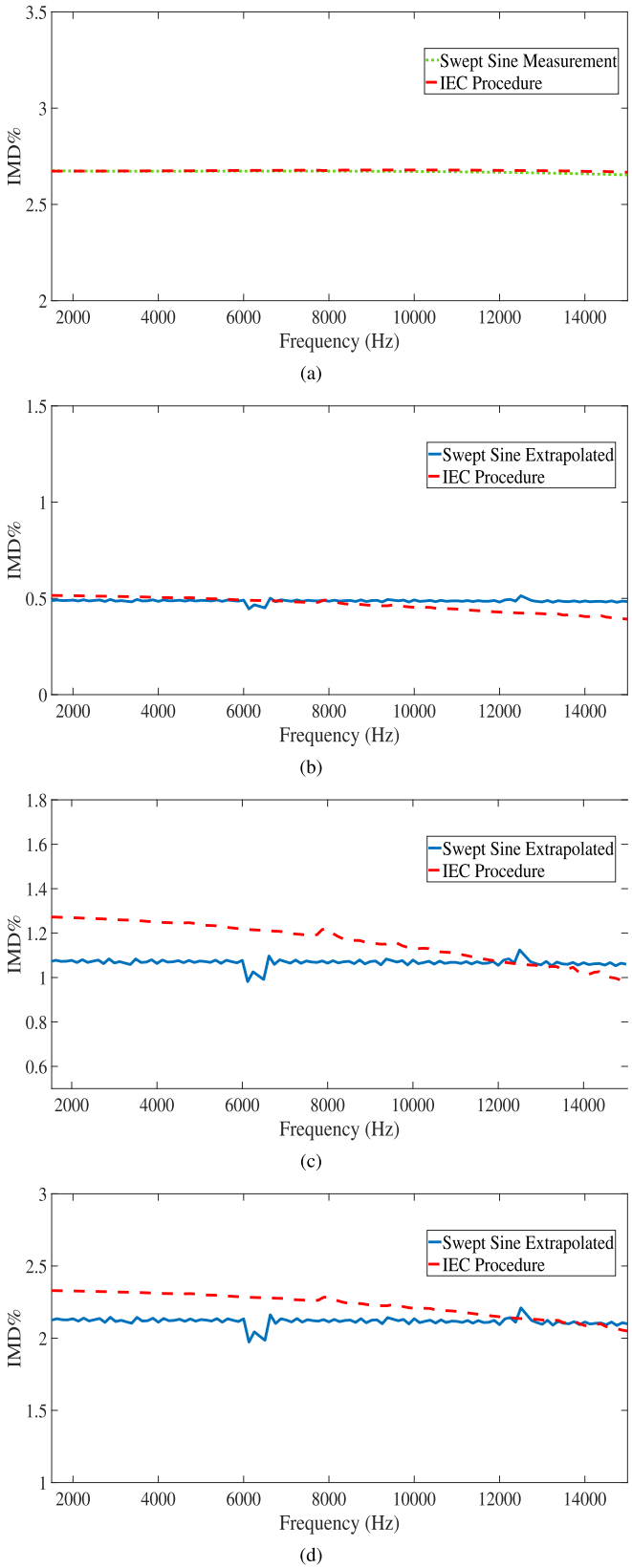

Fig. 9. Estimation results considering an input signal of 1.40 V_{pp} to the tube preamplifier. (a) Estimated curve, (b) with an extrapolation to 0.41 V, (c) with an extrapolation to 0.62 V, and (d) with an extrapolation to 0.93 V.

this can be explained considering that the Fender amplifier has a multistage structure, extremely more complex than the tube preamplifier, so it is reasonable to expect a much more difficult definition of its model.

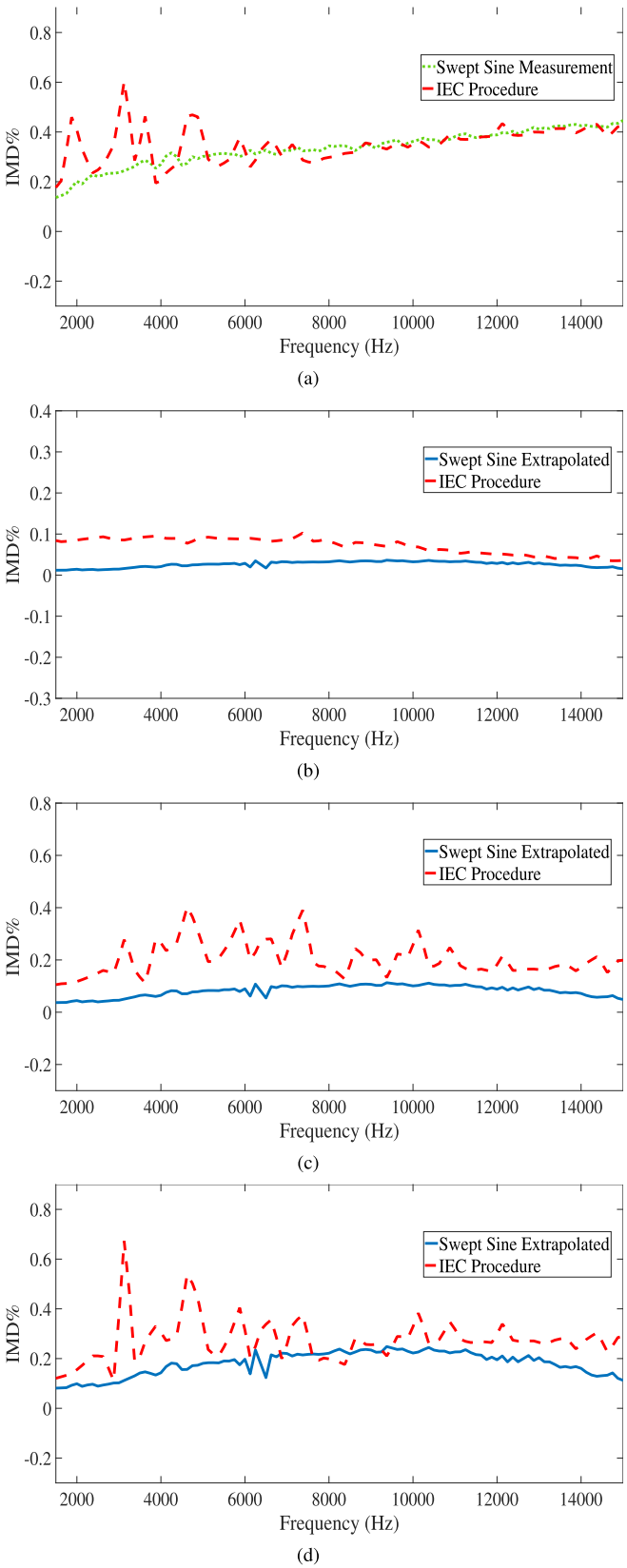

Fig. 10. Estimation results considering an input signal of 0.62 V_{pp} to the guitar amplifier. (a) Estimated curve, (b) with an extrapolation to 0.1 V, (c) with an extrapolation to 0.18 V, and (d) with an extrapolation to 0.28 V.

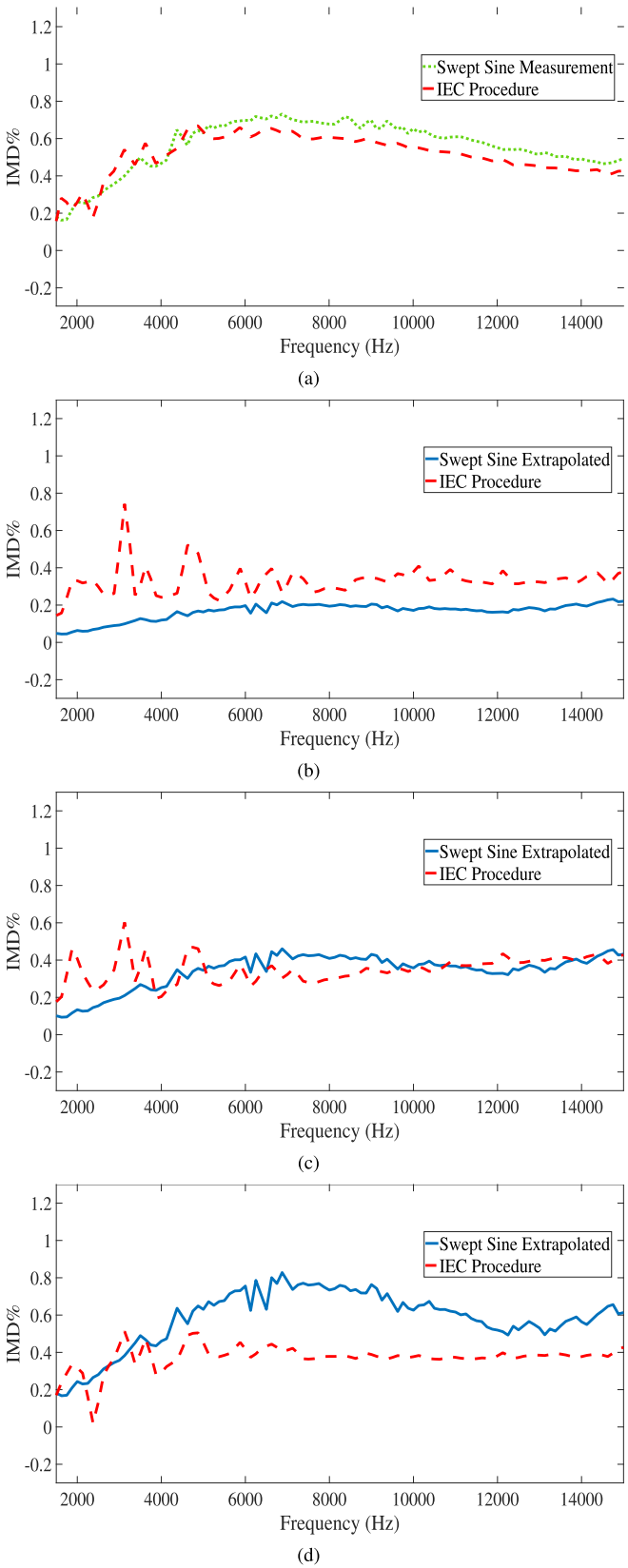

Fig. 11. Estimation results considering an input signal of 1.40 V_{pp} to the guitar amplifier. (a) Estimated curve, (b) with an extrapolation to 0.41 V, (c) with an extrapolation to 0.62 V, and (d) with an extrapolation to 0.93 V.

Regarding the complexity of the proposed approach, an evaluation in terms of measurement execution time has been considered in comparison with the IEC 60 268 procedure. For both the procedures, the requested time has been measured using the same approach based on the *tick count (ms)* function available in Labview. Considering the estimation on the whole

frequency band and for four different amplitudes, we obtain that the IEC measurement took ∼1046.4 s, while the proposed approach requires ∼20 s. This remarkable difference is due to the fact that the IEC measurement requires ∼2.4 s for each frequency value, and 109 measurements have to be performed to cover the useful frequency band, each of them repeated for the four amplitudes. We have to underline that such an advantage of the proposed approach could be significant, especially for some time-critical industrial processes where a measure must be carried out in just a few seconds.

C. Robustness Study

Several tests have been done to evaluate the performance of the algorithm in terms of estimation precision under noisy conditions. For the experiments, the setup shown in Fig. 5 has been considered. A synthetic polynomial nonlinearity and the tube preamplifier of Fig. 2 have been used, considering different signal-to-noise ratios (SNRs).

Focusing on the polynomial, the following nonlinearity has been considered:

$$y = Ax^2 + x^3 \tag{18}$$

where the parameter A allows to vary the amount of quadratic nonlinearity. Since the nonlinearity is defined in analytical form, it is possible to calculate the theoretical third-order IMD, according to the value assigned to the constant A. In this case, its value was set to $A = 0.1125$ as in [31], with an input signal of 1.4-V peak-to-peak amplitude (V_{pp}), leading to a theoretical IMD of 16.7%. Fig. 6 shows the results for three SNR values in terms of frequency behavior of the mean IMD values (blue lines) and confidence intervals (red lines). The plot shows that even in the worst case, the proposed approach is robust and accurate.

For the tube preamplifier, the references are the results shown in Fig. 9(a), which report the measurements without noise addiction. Fig. 7 shows the obtained results with three different SNR levels and with 20 repetitions of each measurement. Also, in this case, the blue lines represent the mean values, while the red dashed lines show the confidence interval for each estimation. As expected, for an SNR of 20 or 30 dB, the estimations are very accurate also with a limited confidence interval, while, in the worst scenario, i.e., an SNR of 10 dB, the measurements still remain good with an acceptable confidence interval confirming the proposed approach robustness against noise.

IV. Conclusion

In this article, we have proposed an original third-order IMD estimation technique that allows to estimate the frequency trend of the $2f_2 - f_1$ distortion from a single detection. In particular, it allows to obtain an estimate of the distortion not only for the signal level actually used in the measurement but also for signal amplitudes other than that, thus extrapolating the estimate of IMD. Several experiments have been carried out on real audio devices and synthetic systems, comparing the results obtainable through the proposed technique with the results deriving from the application of the techniques prescribed by the international standards. The results obtained in the tests carried out on real devices are good, confirming the effectiveness of the proposed approach both in the estimation phase and in the extrapolation of the estimates to a whole range of input signal levels different from the one applied. Finally, a robustness study on synthetic and real systems has underlined the potentiality of the proposed approach in real scenarios under noisy conditions since the methodology has provided good results also in the presence of high noise levels.

References

[1] D. Bard, "Horn loudspeakers nonlinearity comparison and linearization using volterra series," in *Proc. Audio Eng. Soc. Conv. 124*, May 2008, pp. 1–10. [Online]. Available: http://www.aes.org/e-lib/browse.cfm?elib=14448

[2] W. Klippel, "Active compensation of transducer nonlinearities," in *Proc. Audio Eng. Soc. Conf., 23rd Int. Conf., Signal Process. Audio Recording Reprod.*, 2003, pp. 1–17.

[3] Y. H. Lim, Y. S. Cho, I. W. Cha, and D. H. Youn, "An adaptive nonlinear prefilter for compensation of distortion in nonlinear systems," *IEEE Trans. Signal Process.*, vol. 46, no. 6, pp. 1726–1730, Jun. 1998.

[4] J. Pakarinen and D. T. Yeh, "A review of digital techniques for modeling vacuum-tube guitar amplifiers," *Comput. Music J.*, vol. 33, no. 2, pp. 85–100, Jun. 2009.

[5] F. T. Agerkvist, "Volterra series based distortion effect," in *Proc. Audio Eng. Soc. Conv. 129*, Nov. 2010, pp. 1–7. [Online]. Available: http://www.aes.org/e-lib/browse.cfm?elib=15634

[6] F. Eichas, S. Möller, and U. Zölzer, "Block-oriented modeling of distortion audio effects using iterative minimization," in *Proc. 20th Int. Conf. Digit. Audio Effects (DAFx-15)*, Trondheim, Norway, Nov./Dec. 2015, pp. 1–6.

[7] M. Holters, K. Dempwolf, and U. Zölzer, "A digital emulation of the boss sd-1 super overdrive pedal based on physical modeling," in *Proc. Audio Eng. Soc. Conv. 131*, Oct. 2011, pp. 1–10. [Online]. Available: http://www.aes.org/e-lib/browse.cfm?elib=16032

[8] D. T. Yeh, J. Abel, and J. O. Smith, "Simulation of the diode limiter in guitar distortion circuits by numerical solution of ordinary differential equations," in *Proc. 10th Int. Conf. Digit. Audio Effects (DAFx-07)*, Bordeaux, France, Sep. 2007, pp. 1–7.

[9] M. Karjalainen and J. Pakarinen, "Wave digital simulation of a vacuum-tube amplifier," in *Proc. IEEE Int. Conf. Acoust. Speed Signal Process. Proc.*, vol. 5, May 2006, pp. 153–156.

[10] W. R. Dunkel, M. Rest, K. J. Werner, M. J. Olsen, and J. O. Smith, "The fender Bassman 5F6-A family of preamplifier circuits—A wave digital filter case study," in *Proc. 19th Int. Conf. Digit. Audio Effects*, 2016, pp. 263–270.

[11] T. I. Karimov, D. N. Butusov, and A. I. Karimov, "Computer simulation of audio circuits with vacuum tubes," in *Proc. IEEE Int. Conf. Soft Comput. Meas. (SCM)*, May 2016, pp. 114–116.

[12] M. Gasparini, L. Romoli, S. Cecchi, and F. Piazza, "Identification of hammerstein model using cubic splines and FIR filtering," in *Proc. 8th Int. Symp. Image Signal Process. Anal. (ISPA)*, Trieste, Italy, Sep. 2013, pp. 354–359.

[13] L. Romoli, M. Gasparini, S. Cecchi, A. Primavera, and F. Piazza, "Adaptive identification of nonlinear models using orthogonal nonlinear functions," in *Proc. 48th Audio Eng. Soc. Conf.*, Monaco, Germany, Sep. 2012, pp. 1–7.

[14] M. Gasparini, A. Primavera, L. Romoli, S. Cecchi, and F. Piazza, "System identification based on hammerstein models using cubic splines," in *Proc. 134th Audio Eng. Soc. Conv.*, Rome, Italy, May 2013, pp. 1–8.

[15] F. Eichas, E. Gerat, and U. Zölzer, "Virtual analog modeling of dynamic range compression systems," in *Proc. Audio Eng. Soc. Conv. 142*, May 2017, pp. 1–10. [Online]. Available: http://www.aes.org/e-lib/browse.cfm?elib=18628

[16] E. Gerat, F. Eichas, and U. Zölzer, "Virtual analog modeling of a UREI 1176LN dynamic range control system," in *Proc. Audio Eng. Soc. Conv. 143*, Oct. 2017, pp. 1–10. [Online]. Available: http://www.aes.org/e-lib/browse.cfm?elib=19249

[17] S. Orcioni, A. Terenzi, S. Cecchi, F. Piazza, and A. Carini, "Identification of volterra models of tube audio devices using multiple-variance method," *J. Audio Eng. Soc.*, vol. 66, no. 10, pp. 823–838, Oct. 2018.

[18] S. Boyd and L. Chua, "Fading memory and the problem of approximating nonlinear operators with volterra series," *IEEE Trans. Circuits Syst.*, vol. 32, no. 11, pp. 1150–1161, Nov. 1985.

[19] A. Novák, L. Simon, F. Kadlec, and P. Lotton, "Nonlinear system identification using exponential swept-sine signal," *IEEE Trans. Instrum. Meas.*, vol. 59, no. 8, pp. 2220–2229, Aug. 2010.

[20] A. Novak, B. Maillou, P. Lotton, and L. Simon, "Nonparametric identification of nonlinear systems in series," *IEEE Trans. Instrum. Meas.*, vol. 63, no. 8, pp. 2220–2229, Aug. 2014.
[21] A. Farina, A. Bellini, and E. Armelloni, "Non-linear convolution: A new approach for the auralization of distorting systems," in *Proc. 110th Audio Eng. Soc. Conv.*, Amsterdam, The Netherlands, May 2001, pp. 1–4.
[22] M. Rébillat, R. Hennequin, É. Corteel, and B. F. G. Katz, "Identification of cascade of hammerstein models for the description of nonlinearities in vibrating devices," *J. Sound Vib.*, vol. 330, no. 5, pp. 1018–1038, Feb. 2011.
[23] V. J. Mathews and G. L. Sicuranza, *Polynomial Signal Processing*. New York, NY, USA: Wiley, 2000.
[24] T. Schmitz and J.-J. Embrechts, "Hammerstein kernels identification by means of a sine sweep technique applied to nonlinear audio devices emulation," *J. Audio Eng. Soc.*, vol. 65, no. 9, pp. 696–710, Sep. 2017. [Online]. Available: http://www.aes.org/e-lib/browse.cfm?elib=19200
[25] M. Scarpiniti, D. Comminiello, R. Parisi, and A. Uncini, "Comparison of hammerstein and Wiener systems for nonlinear acoustic echo cancelers in reverberant environments," in *Proc. 17th Int. Conf. Digit. Signal Process. (DSP)*, Jul. 2011, pp. 1–6.
[26] A. Terenzi, V. Bruschi, S. Cornell, A. Castellani, and S. Cecchi, "A multiband structure based on hammerstein model for nonlinear audio system identification," in *Proc. 11th Int. Symp. Image Signal Process. Anal. (ISPA)*, Sep. 2019, pp. 9–14.
[27] F. Eichas, S. Möller, and U. Zölzer, "Block-oriented gray box modeling of guitar amplifiers," in *Proc. 20th Int. Conf. Digit. Audio Effects (DAFx)*, Edinburgh, U.K., Sep. 2017, pp. 184–191.
[28] E.-P. Damskägg *et al.*, "Real-time modeling of audio distortion circuits with deep learning," in *Proc. Int. Sound Music Comput. Conf. (SMC)*, Malaga, Spain, 2019, pp. 332–339.
[29] M. A. M. Ramírez and J. D. Reiss, "Modeling nonlinear audio effects with end-to-end deep neural networks," in *Proc. IEEE Int. Conf. Acoust., Speech Signal Process. (ICASSP)*, May 2019, pp. 171–175.
[30] J. Vanderkooy and S. P. I. Thomson, "Harmonic distortion measurement for nonlinear system identification," in *Proc. 140th Audio Eng. Soc. Conv.*, Paris, France, Jun. 2016, pp. 1–11.
[31] P. Burrascano *et al.*, "A swept-sine pulse compression procedure for an effective measurement of intermodulation distortion," *IEEE Trans. Instrum. Meas.*, vol. 69, no. 4, pp. 1708–1719, Apr. 2020.
[32] T. J. Rivlin, *Chebyshev Polynomials*. New York, NY, USA: Dover, 2020.
[33] A. Farina, "Simultaneous measurement of impulse response and distortion with a swept-sine technique," *J. Audio Eng. Soc.*, no. 5093, pp. 1–23, Feb. 2000.
[34] P. Burrascano, S. Laureti, and M. Ricci, "Accuracy analysis of harmonic distortion estimation through exponential chirp pulse compression," in *Proc. Int. Conf. Control, Autom. Diagnosis (ICCAD)*, Jul. 2019, pp. 1–6.
[35] National Instruments. (2017). *Sound and Vibration Toolkit*. [Online]. Available: https://www.ni.com/trysv/
[36] *Sound System Equipment—Part 3: Amplifiers*, International Standard IEC 60268-3, 2003.
[37] National Instruments. (2008). *Pxie-4461 DSA Dynamic Signal Acquisition Device*. [Online]. Available: http://www.ni.com/pdf/manuals/373770j.pdf

Pietro Burrascano was worked with the General Headquarters of Telespazio SpA, Fucino, Ortucchio, Italy, from 1981 to 1983, dealing with the planning of satellite telecommunications systems. In 1984, he joined the Info-Com Department, University of Rome "Sapienza," Rome, Italy, as a Researcher. Since 1994, he has been a Full Professor of electrical engineering with the University of Perugia, Perugia, Italy, where he was the Deputy-Rector from 2002 to 2014. From 2007 to 2013, he was the Chairman of the National Coordination Group of Researchers in electrical engineering. From 2016 to 2020, he was the Coordinator of the H2020 Marie Skłodowska-Curie European Training Network Project "NDTon-AIR" from 2016 to 2020, a training network in the field of nondestructive testing and state monitoring of aircraft structures. In 2020, he was the Coordinator of the Ph.D. degree in industrial and information engineering with the University of Perugia, from September 2020 to March 2021, and the Head Bachelor and M.Sc. curriculum on Industrial Engineering of Perugia University. He has been the Coordinator of several national and international applied research groups and projects. He has authored more than 140 indexed scientific articles and book chapters in the field of signal and image processing and nondestructive testing and evaluation.

Alessandro Terenzi was born in Senigallia, Italy, in 1991. He received the Laurea degree (Hons.) in electronic engineering and the Ph.D. degree in electronic engineering from the Polytechnic University of Marche, Ancona, Italy, in July 2016 and March 2021, respectively.

He is currently a Post-Doctoral Researcher with the Department of Information Engineering (DII), Polytechnic University of Marche. His current research interests are in the area of digital signal processing, including nonlinear audio systems and audio processing.

Dr. Terenzi is a member of the Acoustic Engineering Society (AES).

Stefania Cecchi (Member, IEEE) was born in Amandola, Italy, in 1979. She received the Laurea degree (Hons.) in electronic engineering from the University of Ancona, Ancona, Italy (now University Politecnica delle Marche, Ancona), in 2004, and the Ph.D. degree in electronic engineering from the University Politecnica delle Marche, Ancona, in 2007.

She was a Post-Doctoral Researcher with the Department of Information Engineering (DII) from February 2008 to October 2015, and an Assistant Professor from November 2015 to October 2018, where she has been an Associate Professor since November 2018. She has authored or coauthored several international articles. Her current research interests are in the area of digital signal processing, including adaptive digital signal processing (DSP) algorithms and circuits, speech, and audio processing.

Dr. Cecchi is a member of the Acoustic Engineering Society (AES) and the Italian Acoustical Association (AIA).

Matteo Ciuffetti received the master's degree in industrial engineering from the University of Perugia, Perugia, Italy, in 2020, where he is pursuing the Ph.D. degree in engineering.

His research activities are focused on linear and nonlinear modeling techniques with applications to nondestructive testing and evaluation.

Susanna Spinsante (Senior Member, IEEE) received the Ph.D. degree in electronics and telecommunications engineering from the Università Politecnica delle Marche, Ancona, Italy, in 2005.

She is currently a Tenure-Track Assistant Professor in electrical and electronic measurements with the Information Engineering Department (DII), Università Politecnica delle Marche, where she spent several years working in signal processing for telecommunications and video applications. Since 2012, her research interests are focused on the use of depth and wearable sensors for the extraction of measurement signals applied to human monitoring, motion-related measurements, action recognition, and their processing by compressed sensing. She has coauthored more than 190 articles in international peer reviewed journals and conference proceedings.

Dr. Spinsante is a member of the IEEE Instrumentation and Measurement Society, the IEEE Signal Processing Society, the Gruppo Misure Elettriche ed Elettroniche (GMEE), and Consorzio nazionale interuniversitario per le telecomunicazioni (CNIT). She is the Chair of the "RGB-D Sensors" Technical Committee of the IEEE Sensors Italy Chapter.